CHAPTER 8

Modelling Shoaling Directional Wave Spectra in Shallow Water

James T. Kirby[1]

Abstract

This paper describes the development of a model for the shoaling and refraction of an incident directional spectrum over beach topography. The present model is limited to topography which varies only in the on- offshore direction, but no restriction is made on allowed angles of incidence with respect to the shore-normal direction. The model is verified in comparison to laboratory data for Mach reflection of cnoidal waves from a vertical plane wall. It is shown that the model provides a more accurate representation of the evolving wave field than does an earlier parabolic approximation, using the same laboratory data.

Introduction

As ocean surface waves propagate towards shore, they pass through a shoaling zone prior to breaking in which nonlinear interactions become strong and can significantly modify the wave train. This zone is characterized by weak frequency dispersion, since waves become relatively long compared to local water depth. In addition, the weak dependence on wavelength in the wave phase speed leads to the occurrence of strong nonlinear interactions at second-order in wave height. The combined effects of weak dispersion and nonlinearity may be modelled by the Boussinesq equations, which serve as a reasonably accurate general purpose model for the domain in question as long as waves do not become too high.

Since the area being studied here can be quite extensive in comparison to the characteristic wavelength of the waves being modelled, the choice of an efficient numerical solution technique is crucial. The Boussinesq equations may be successfully solved by time-stepping techniques, but these methods are too inefficient for the spatial and temporal spans being considered in applications to an open coastal zone. Instead, various prior studies have found that it is efficient to decompose the time-dependent wave train into a stack of frequency components by Fourier decomposition, and then solve for the spatial evolution of each frequency mode. This is exactly the same kind of manipulation that is done in Fourier analysis of data, and is valid as long as the wave train satisfies the requirements for the transform to exist. In field applications, the Fourier decomposition into a finite set of discrete frequencies under the assumption of periodicity is exactly the same as applying an FFT to data. Assumptions about stationarity of the

[1]Center for Applied Coastal Research, Department of Civil Engineering, University of Delaware, Newark, Delaware 19716

process are implicit and should be kept in mind when determining if the present approach is useful.

The solution for the spatial behavior of each frequency component is itself involved. A number of studies (Freilich and Guza, 1984; Elgar and Guza, 1985 and 1986 and subsequent contributions) have considered only the shoreward propagation in one space dimension, and have shown that the resulting one-dimensional, first-order coupled mode equations are capable of modelling the evolution of the spectrum and bispectrum of shoaling waves, as verified by comparison with field measurements. Liu, Yoon and Kirby (1985; referred to here as LYK) alternately proposed a parabolic model for the shoreward propagation of each frequency component over two-dimensional topography, and verified the method in comparison to a laboratory experiment on the focussing of periodic long waves by topography. The parabolic model approach has also been used to study a field application (Freilich et al, 1990), with successful results.

In this study, we derive a model for the evolution of each frequency mode in two dimensions, based on the angular spectrum approach. This approach has been applied to the study of intermediate depth waves by Dalrymple and Kirby (1988) and Dalrymple et al (1989). For the case of linear theory, the angular spectrum is usually posed as the continuous Fourier transform of the wave field in the longshore direction. Here, in keeping with the mental framework associated with the discrete transforms being employed in time, we impose longshore periodicity as well and obtain a discrete spectrum in longshore wavenumber. This frequency - longshore wavenumber spectrum is subsequently referred to as the *discrete angular spectrum.*

The model developed here is applicable both to simple periodic waves generated in the laboratory environment and to irregular, "random" waves in the field environment. In this paper, we concentrate on a model verification conducted from the first viewpoint. The model is tested against laboratory data obtained by Hammack, Scheffner and Segur (1990), who investigated the development of a Mach stem arising during the glancing-angle reflection of a cnoidal wave by a vertical wall. Results obtained using the parabolic equation model described in LYK are also compared to data. (The case of Mach reflection of a cnoidal wave has been studied using the parabolic approximation by Yoon and Liu (1989); however, no comparison to data was provided in that study.) The spectral model is shown to give a more accurate representation of the data than the parabolic model over the entire range of angles of incidence considered.

The Boussinesq Equation Model

We first establish the form of a model for waves in a laterally unrestricted domain. A Cartesian coordinate system is adopted which has x pointed in the onshore direction and y pointing alongshore. Depth is assumed to vary as $h(x)$ only. We take as a starting point the variable depth Boussinesq equations as given by Peregrine (1967):

$$\eta_t + \nabla \cdot (h\mathbf{u}) + (\epsilon)\nabla \cdot (\eta \mathbf{u}) = 0 \tag{1}$$

$$\mathbf{u}_t + (\epsilon)\mathbf{u} \cdot \nabla \mathbf{u} + g\nabla\eta = (\mu^2)\{\frac{h}{2}\nabla(\nabla \cdot (h\mathbf{u}_t)) - \frac{h^2}{6}\nabla(\nabla \cdot \mathbf{u}_t)\} \tag{2}$$

Here, η is the surface displacement and $\mathbf{u}$ is the horizontal wave- induced velocity. The equations are kept in dimensional form; the scaling parameters $\epsilon = \max(\eta)/h$ for nonlinearity and $\mu^2 = \omega^2 h/g$ for weak dispersion are present only schematically and will be subsequently dropped. We will assume that either bottom slope

or the amplitude of bottom features (as scaled by water depth) are also small and hence the model will be developed to leading order in nonlinearity, dispersion, and domain inhomogeneity. This leads to immediate neglect of bottom slope effects in the dispersive terms of (2). Using the linear portion of (1), we may then write (2) in the reduced form

$$\mathbf{u}_t + \mathbf{u} \cdot \nabla \mathbf{u} + g\nabla\eta + \frac{h}{3}\nabla\eta_{tt} = 0. \tag{3}$$

We now make the following assumptions. First, the model will be applied to time-periodic wave trains, where periodicity is in the sense of either a regular wave train, or of a discrete FFT over a finite length of sampled data. Secondly, the wave field will be assumed to be periodic in the transverse y direction. This corresponds again to a fixed longshore wavelength in the regular wave case, or to periodicity over a long spatial interval in the spectral sense.

The governing equations are first split into coupled elliptic models for separate harmonic components. Following LYK, we write the surface displacement and velocity as

$$\eta = \sum_{n=0}^{N} \frac{\eta_n(x,y)}{2} e^{-in\omega t} + c.c. \tag{4}$$

$$\mathbf{u} = \sum_{n=0}^{N} \frac{\mathbf{u}_n(x,y)}{2} e^{-in\omega t} + c.c. \tag{5}$$

Substitution of (4) and (5) in (1) and (3) and subsequent elimination of the velocity leads to the following model equation for the η_n in the horizontal plane:

$$n^2\omega^2\eta_n + \nabla \cdot (G_n \nabla \eta_n) + [n.l.t.]_n = 0; \qquad n = 1, ..., N \tag{6}$$

Here, $[n.l.t]_n$ denotes the nonlinear interactions with other discrete frequency components which are sorted by means of the rules for triad interactions applied to the time dependence. (Omitted details may be found in the more complete paper; Kirby (1990).) The mode $n = 0$ corresponding to the steady, wave-induced setdown is neglected since it is at most second order in the largest wave amplitudes present (see LYK). Also,

$$G_n(x) = gh(x) - \frac{1}{3}n^2\omega^2 h^2(x). \tag{7}$$

We now apply a spectral transform to the y dependence of the wavefield, assuming propagation is to be considered in the on-offshore ($\pm x$) direction. We consider here the case of an unbounded lateral domain and a wavefield which is periodic over the basic interval L. We then represent $\eta_n(x,y)$ as

$$\eta_n(x,y) = \sum_{m=-M}^{M} \eta_n^m(x) e^{im\lambda_0 y} \tag{8}$$

where

$$\lambda_0 = \frac{2\pi}{L}. \tag{9}$$

Substituting (8) in (6) and neglecting x - derivatives of small terms in G_n then leads to a set of coupled second-order ODE's for the η_n^m, given by

$$\frac{G_n}{gh}\eta_{n,xx}^m + \frac{h_x}{h}\eta_{n,x}^m + (\gamma_n^m)^2\eta_n^m + \frac{1}{3}m^2n^2\lambda_0^2k^2h^2\eta_n^m + \frac{1}{gh}[n.l.t.]_n^m = 0;$$
$$n = 1,...,N; \qquad m = -M,...,M. \tag{10}$$

where $[n.l.t.]_n^m$ now represents triad interactions satisfying resonance conditions in t and y. Here, k is the wavenumber determined by the lowest order dispersion relation

$$\omega^2 = gk^2h. \tag{11}$$

Also,

$$(\gamma_n^m)^2 = n^2k^2 - m^2\lambda_0^2 \tag{12}$$

For fixed n, k, λ_0, large values of m will make γ_n^m imaginary, which corresponds to modes which are exponential rather than oscillatory in x in the linear approximation. In the linear case, the presence of these modes in the initial conditions would be interpreted in the same light as the presence of evanescent modes in the general wavemaker problem (see Dalrymple and Kirby, 1988). However, the interpretation in the case of possible nonlinear forcing of the offshore portion of trapped modes in the nearshore region is non-trivial and will need to be considered carefully in applications where the inclusion of this effect is desired. In addition, nonlinearity could force the propagation of modes that would not be present in a linearized wave field, and which could affect a detailed representation of an individual wave. At present, the range of M at each value of n may be restricted to $M_n \leq nk/\lambda_0$ in order to eliminate forcing of these modes arbitrarily.

Shoaling Waves

Based on the linear, nondispersive portion of the model (10), we assume that the incident wave may be written in the form

$$\eta_n^m(x) = A_n^m(x)e^{in\int k\tilde{\gamma}_n^m dx} \tag{13}$$

where it is assumed that the x dependence of A, k and $\tilde{\gamma}$ is on a slow scale of $O(\epsilon)$, and where

$$\tilde{\gamma}_n^m = (1 - (\frac{m}{n})^2(\frac{\lambda_0}{k})^2)^{1/2} = \frac{\gamma_n^m}{nk} \tag{14}$$

(where the positive root is taken). The amplitudes A represent the discrete angular spectrum being considered here, and are allowed to vary owing to refraction, shoaling, dispersion and nonlinear interaction. (It would be possible to absorb shoaling and refraction effects by the use of the usual linear refraction formulae; this step is not taken here.) Substitution of (13) in (10) leads to the spectral model for incident waves, given by

$$\tilde{\gamma}_n^m A_{n,x}^m + \frac{(kh\tilde{\gamma}_n^m)_x}{2kh}A_n^m - \frac{1}{6}in^3k^3h^2A_n^m + +\frac{ink}{8h}\left\{\sum_{l=1}^{n-1}\sum_{p=P_1}^{P_2} I_{n,l}^{m,p}A_l^pA_{n-l}^{m-p}e^{i\int\Theta_{n,l}^{m,p}dx}\right.$$
$$\left. +2\sum_{l=1}^{N-n}\sum_{p=P_3}^{P_4} J_{n,l}^{m,p}A_l^{p*}A_{n+l}^{m+p}e^{i\int\Upsilon_{n,l}^{m,p}dx}\right\} = 0;$$
$$n = 1,...,N; \qquad m = -M_n,...,M_n. \tag{15}$$

Here, $(\cdot)^*$ denotes the complex conjugate. The limits of summation $P_1 - P_4$ are determined by the range of allowed modes taking part in each interaction. The interaction coefficients I and J are given by

$$I_{n,l}^{m,p} = 1 + [\tilde{\gamma}_l^p \tilde{\gamma}_{n-l}^{m-p} + \frac{p}{l}\frac{m-p}{n-l}(\frac{\lambda_0}{k})^2] \cdot [1 + (\frac{m}{n})^2(\frac{\lambda_0}{k})^2 + \frac{(l\tilde{\gamma}_l^p + (n-l)\tilde{\gamma}_{n-l}^{m-p})^2}{n^2}] \quad (16)$$

$$J_{n,l}^{m,p} = I_{n,-l}^{m,-p}. \quad (17)$$

The phase arguments Θ and Υ represent the basic mismatch in the x direction of the triads chosen based on perfect matching in y and t. Generally, the only components which experience complete resonance in the long wave limit must have parallel propagation directions; all obliquely interacting components are somewhat detuned. The phase arguments are given by

$$\Theta_{n,l}^{m,p} = lk\tilde{\gamma}_l^p + (n-l)k\tilde{\gamma}_{n-l}^{m-p} - nk\tilde{\gamma}_n^m \quad (18)$$

$$\Upsilon_{n,l}^{m,p} = \Theta_{n,-l}^{m,-p} \quad (19)$$

The spectral model (15) is a set of coupled first order ODE's which are solvable by standard techniques. Results presented in sections 4 and 5 were obtained using a standard 4th-order Runge-Kutta scheme with fixed step size and no error checking. Presently, extensions of the model using error control and adaptive step size are being tested and will likely be the vehicle for further field testing of the model beyond the scope of the present study.

Comparison with Data and a Parabolic Model Approximation

In order to verify the basic computational model provided by (15) and to test whether the present angular spectrum provides a more accurate representation of the wave field relative to earlier parabolic models (LYK; Yoon and Liu, 1989), we have compared model predictions to laboratory data obtained by Hammack et al (1990) for the case of glancing, or Mach, reflection of a cnoidal wave by a vertical wall. The experimental tests were conducted using the directional wave maker at the Coastal Engineering Research Center, Vicksburg, MS. A prior use of this facility to study the properties of intersecting cnoidal waves is described in Hammack et al (1989), referred to here as HSS.

Layout of Experimental Facility

For the tests considered here, the wave basin was operated with a water depth of $20cm$ in a constant depth region extending $12.55m$ in front of the wavemaker, after which a beach with 1:30 slope provided an efficient wave absorber giving little reflection. The basin floor was leveled to a tolerance of $0.01ft$ in order to remove some of the spatial irregularity of the waves reported in HSS resulting from local refraction effects. For the Mach stem tests, two parallel false walls were installed perpendicular to the wavemaker axis in order to provide a closed channel. The channel walls were situated $13.26m$ apart, which fixes the width of the numerical domain to be considered.

Instrumentation and data aquisition are described in HSS, and readers are referred there for greater detail. In the present tests, an array of 18 wave gages

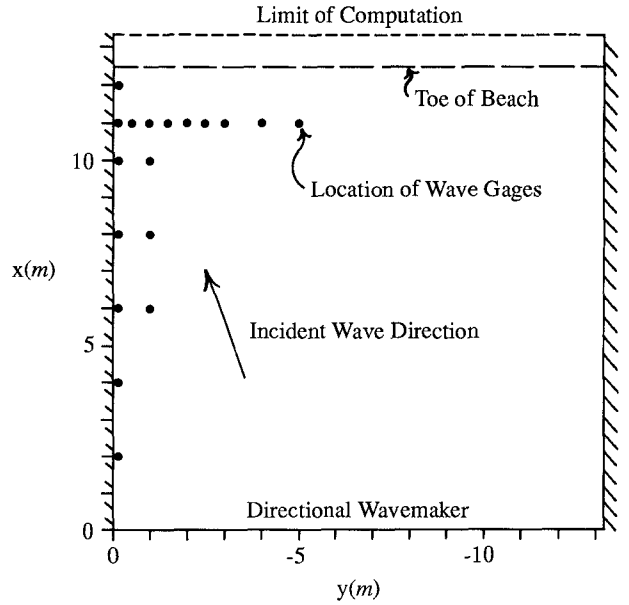

Figure 1: Basin configuration, Mach reflection experiments

were installed in the basin as shown in Figure 1. In this figure, the directional wavemaker occupies the y-axis, and the channel sidewalls lie along the x-axis and the line $y = -13.26m$. The positions of the gages are given in Table 1. The linear gage array $13-9-8-7-6-4-3-2-1$ provides a transect perpendicular to the reflecting sidewall which allows a determination of the width and structure of the Mach stem and additional crests in the reflection pattern. This array is used to provide most of the information described below. An additional array $18-17-16-15-14-13-5$ provides measurements of the evolution of the reflected stem wave along the wall. For each gage, data consists of a time series of 1250 points with a sampling rate of $25Hz$.

gage	$x(m)$	$y(m)$	gage	$x(m)$	$y(m)$	gage	$x(m)$	$y(m)$
1	11	-5	7	11	-1.5	13	11	-0.07
2	11	-4	8	11	-1	14	10	-0.07
3	11	-3	9	11	-0.5	15	8	-0.07
4	11	-2.5	10	8	-1	16	6	-0.07
5	12	-0.07	11	6	-1	17	4	-0.07
6	11	-2	12	10	-1	18	2	-0.07

Table 1: Wave gage positions in Mach reflection experiments

test	CR15	CR22	CR30	CR38	CR48	CR58
α	14.5	22.0	30.0	38.5	47.5	57.6
β	10.13	15.48	21.34	27.84	35.18	44.32

Table 2: Paddle phase angles and directed wave angles; Mach reflection experiments

Specification of the Incident Wave

The generation of oblique cnoidal waves using the directional wavemaker has been described in HSS. In the present laboratory tests, waves were initially specified as having a wavelength of $2m$ and a crest elevation $4cm$ above mean water level. The algorithms given by Goring and Raichlen (1980) were used to generate a time series of paddle displacement corresponding to one- dimensional generation. Oblique waves were then generated by phase lagging adjacent paddles. The relation between paddle phase shift angle β and directed wave angle α is given by

$$\beta = \arcsin(\alpha L/360W) \tag{20}$$

where L is the wave length and $W = 45cm$ is the individual paddle width. Tests were conducted for six paddle phase lags, and are denoted $CRxx0204$, where xx denotes paddle phase lag. Note that (48) corrects a typographic error appearing in HSS. Table 2 gives a list of α and β values for the six tests.

Prior to running the Mach reflection experiments, the nominally $4cm$ high wave was generated in the normally incident direction (traveling parallel to sidewalls) in order to study its characteristics. It was found that the wave actually had a crest elevation close to $3.3cm$ above mean water level. This value was used to specify incident waves in the numerical computation, along with a wave period of $1.478s$ as specified by KdV cnoidal wave theory. We note that it is uncertain whether the value of $3.3cm$ was invariant under changes of angle of incidence in the laboratory experiment. Variation of this quantity would add an untraceable source of error in model-data comparison.

The computed wave angle and the Fourier coefficients for the input cnoidal wave were used to compute the surface displacement for oblique cnoidal waves along the boundary $x = 0m$ corresponding to the wavemaker. For parabolic model calculations, information in the range $-13.26m \leq y \leq 0m$ was used to start the computation. The model was run with reflective sidewalls at $y = 0, -13.26m$. For the spectral model, a periodic interval was constructed by using a mirror image about $y = 0m$; the computational domain thus corresponds to the region $-13.26m \leq y \leq 13.26m$. The computed waveform was then Fourier transformed over this interval and the resulting frequency-wavenumber spectrum was fed into the spectral model. (It is noted that the problem as stated could be handled directly by means of a cosine transform over the true model domain; this was not done because of the reprogramming of the basic model that would have been required.)

For the examples shown here, the parabolic model was run with a grid spacing $\Delta x = \Delta y = 0.0625m$, and $N = 9$ frequency components were used. Tests were performed for two cases for both half the grid spacing and twice the number of harmonics to insure that convergence was adequate for the parameters finally used. In the spectral model, we used $N = 9$ and $M = 64$. The large value of M insures that all freely propagating modes of the solution are retained for the highest harmonic considered. The forward grid space step was also $\Delta x = 0.0625m$. Again, these parameters were found to give sufficient convergence of solutions

when compared to runs with smaller grid steps and more retained frequency components.

Results

Results of model calculations are presented here in two forms: gray level contour plots of instantaneous surface over the model basin, and time series computed from model output and compared to experimental data. The gray level plots are actually of the quantity $-\partial\eta/\partial x$, and the pictures thus mimic the visual image that would be obtained in an overhead photograph resulting from lighting at a low angle from the direction of the wavemaker. (This is similar to the photographic arrangement in HSS). In all cases, the gray level plots from parabolic model computations are similar to those from spectral model computations, and only spectral model results are shown. Figure 2 presents results for the test CR150204, which clearly shows the evolution of a wide Mach stem wave along the reflecting boundary. In contrast, the wave field for test CR580204, where the angle of incidence is about 45°, exhibits almost a regular (i.e., linear) reflection pattern consisting of superposed waves (Figure 3).

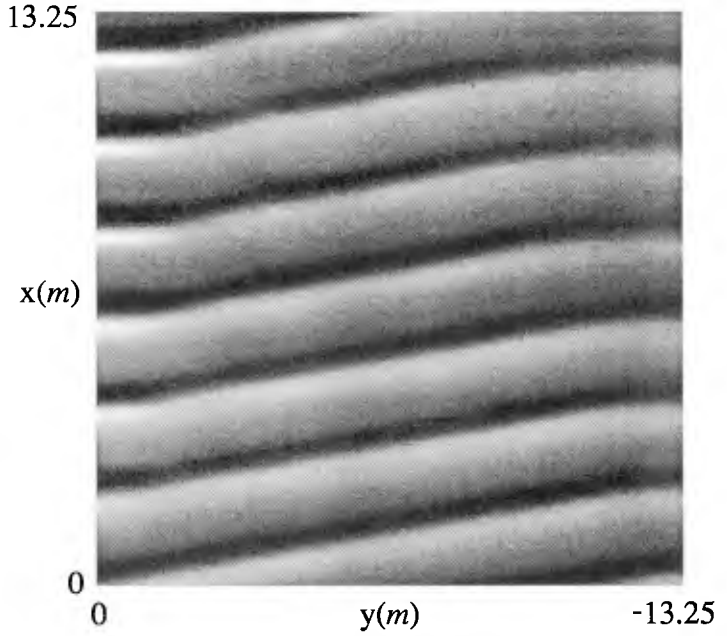

Figure 2: Predicted wave field, test CR150204. Spectral model

In order to compare time series from experiment and model calculations, the

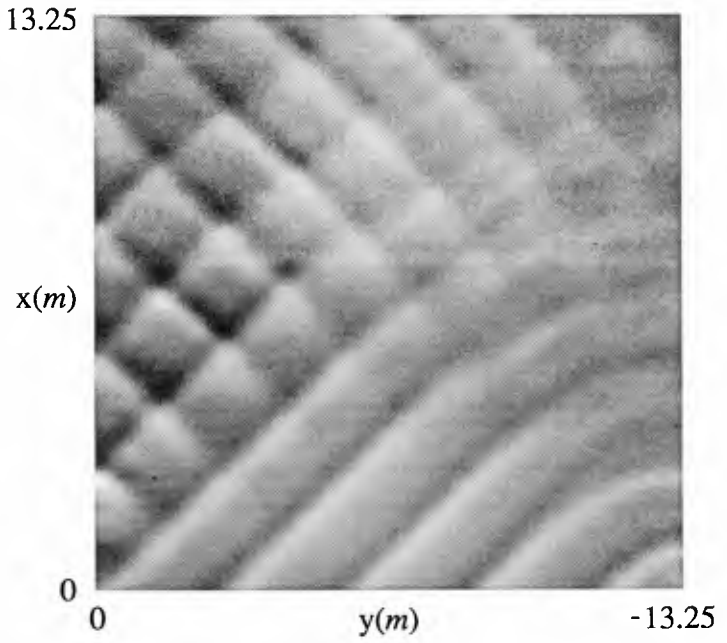

Figure 3: Predicted wave field, test CR580204. Spectral model

following procedure is used. First, after allowing some time for nearly periodic motion to be established in the experiment, a reference time t_0 is established at the position of a wave crest at gage 13 ($x = 11m, y = -0.07m$). This start time is used for all other gages as well, in order to maintain synchronization. Then, a start time is also established for the model- predicted time series by identifying a crest at model gage 13. Synchronization between model and data time series is thus based on correlating the series at a gage location, rather than (more correctly) correlating at the wavemaker. This step is necessary since the wavemaker control is not available and since absolute time in the model-constructed time series is arbitrary.

After determining the synchronous start times for model and data at gage 13, time series were plotted for the transect along the wall (gages 18-17-16-15-14-13-5) and perpendicular to the wall (gages 13-9-8-7-6-4-3-2-1). Aside from the presence of experimental errors, a correct model result would be indicated by complete agreement between model and data time series at each gage. As examples, two periods of time series for the perpendicular transect are shown in Figure 4 for the spectral model predictions for CR150204. The plot shows a stem developed near the wall in the area spanned by gages 13-9-8-7, beyond which there is a clear phase lead at each subsequent gage, indicating the approach of

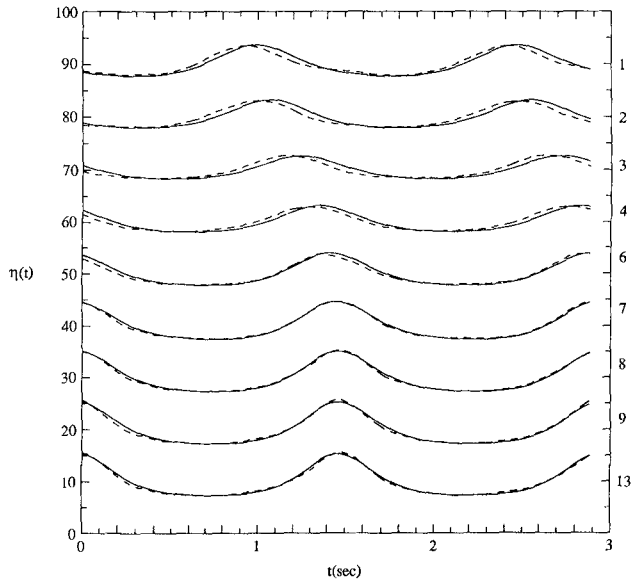

Figure 4: Measured and predicted time series for test CR150204, perpendicular transect. ——, model; - - -, data. Spectral model

the incident wave at a small angle of incidence. In this plot, model predictions are indicated by solid lines and experimental data by dashed lines. At the opposite extreme, Figure 5 shows spectral model predictions and data for the case CR580204. This figure indicates the structure of a short crested wave field, with one complete diamond over the range of gages 13-9-8-7-6-4-3, whereas the signal in gages 3-2-1 indicating a strong progressive phase lag, corresponding to a wave travelling *away from* the wall at close to 45°. The structure of the plots in Figures 4 and 5 may be further clarified by comparison with the surface plots in Figures 2 and 3, respectively.

In order to quantify the comparison between model predictions and measurements, an rms error measure was constructed. This measure e is given by

$$e_j = \sqrt{\frac{\frac{1}{I}\sum_{i=1}^{I}(\eta_{2,j}(i) - \eta_{1,j}(i))^2}{\frac{1}{I}\sum_{i=1}^{I}(\eta_{1,j}(i))^2}} \tag{21}$$

for each gage, where the normalization of the mean square error is with respect to the true (data) standard deviation. A composite value $\overline{e}$ for each angle or test is constructed from the ratio of the rms error for all points divided by the total

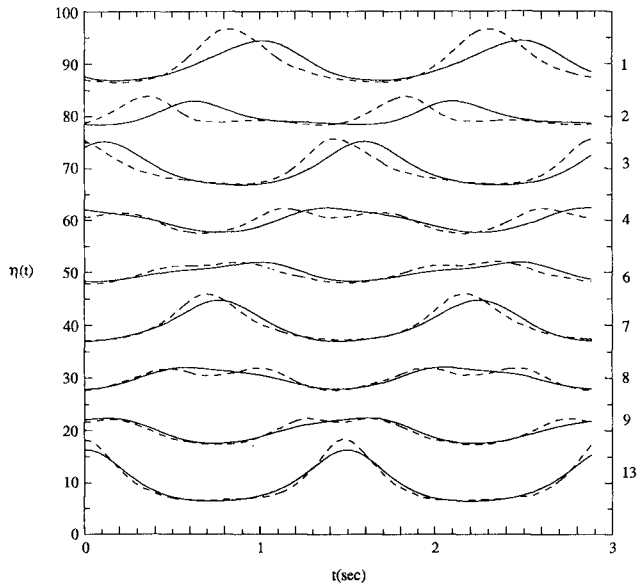

Figure 5: Measured and predicted time series for test CR580204, perpendicular transect. ——, model; - - -, data. Spectral model

standard deviation for all points. Table 3 gives the computed error estimates for all tests, and Figure 6 shows the composite error as a function of incidence angle for the two models. In this case, the trend towards increasing error with increasing angle is clear in the parabolic model results. The spectral model also shows an increasing trend in this case, which would not necessarily be expected.

One possible reason for an increase in error in the spectral model as wave angle becomes large rests in the fact that the reflected wave crests at the wall and in the short-crested wave pattern away from the wall result from the interaction between waves that are colliding head on to the same extent as they are interacting colinearly. Tests and analysis of head on collision and vertical wall reflection of solitary waves have indicated that the leading order theory (as in the Boussinesq model employed here) is not capable of predicting the height of the runup or maximum elevation, or the phase lag associated with the opposite-going interaction. See Su and Mirie (1980) for an example of this type of analysis. Effects of this nature may be present in the experiments being considered here. It is also possible that the increase in error with incidence angle in the spectral model is due to a change in the incident wave height with angle, as mentioned above. This error, if present, would tend to increase the wave height with angle,

spectral model										
gage	13	9	8	7	6	4	3	2	1	average
CR15	.089	.109	.078	.076	.177	.296	.386	.349	.285	.193
CR22	.228	.292	.281	.305	.326	.496	.346	.148	.526	.296
CR30	.208	.234	.168	.214	1.250	.306	.317	.124	.196	.250
CR38	.276	.535	.578	1.060	.206	.275	.442	.520	.190	.383
CR48	.128	.137	.636	.206	.216	.524	.953	.162	.124	.273
CR58	.194	.277	.479	.293	.540	.717	.631	1.280	.612	.540
parabolic model										
gage	13	9	8	7	6	4	3	2	1	average
CR15	.113	.132	.093	.103	.327	.600	.713	.503	.422	.319
CR22	.191	.326	.407	.556	.916	1.240	.678	.370	1.020	.509
CR30	.242	.225	.418	.597	1.975	.386	.231	.690	.333	.365
CR38	.211	.324	.706	1.936	.430	.550	.612	.713	.489	.494
CR48	.513	.743	1.911	.473	.398	.799	1.425	.476	.598	.599
CR58	.261	.534	1.099	.969	1.611	.630	.672	.697	.515	.689

Table 3: RMS error coefficients $\overline{e}$ for spectral and parabolic model runs

contributing to the deviation between model results and data in the expected way.

Discussion

We have described the development of a solution technique for the Boussinesq model of long waves, based on a discrete representation of the angular spectrum for waves incident towards shore from the ocean. The model is similar in intent to the parabolic model developed earlier by LYK, with the exception that the present model does not impose a restriction on the range of directions that can be accurately modelled. This advantage is counterbalanced (at this stage of development) by the need to impose periodic boundary conditions on the modelled problem. This restriction must be alleviated before the various representations of angular spectrum models (present model; Dalrymple and Kirby, 1988; Dalrymple et al, 1989) become generally applicable as coastal wave models.

Comparison of the present model, a parabolic model and laboratory data indicates that differences do occur between predictions of a small-angle approximation and the fully directional expansion employed here, and that the deviation is apparent even at small angles of incidence. This result indicates that the further development of the angular spectrum model is worth pursuing as a means of providing accurate prediction of coastal wave fields. The first extension of the present model to include weak longshore topographic variation and on-offshore reflection is presently underway and will be described shortly.

Acknowledgements

The author would like to thank the Office of Naval Research for support for this study through grants N00014-89-J-1717 and N00014-90-J-1678, and Joe Hammack, Norm Scheffner and Harvey Segur for their very generous donation of experimental data prior to their own analysis or publication of it. James Kai-

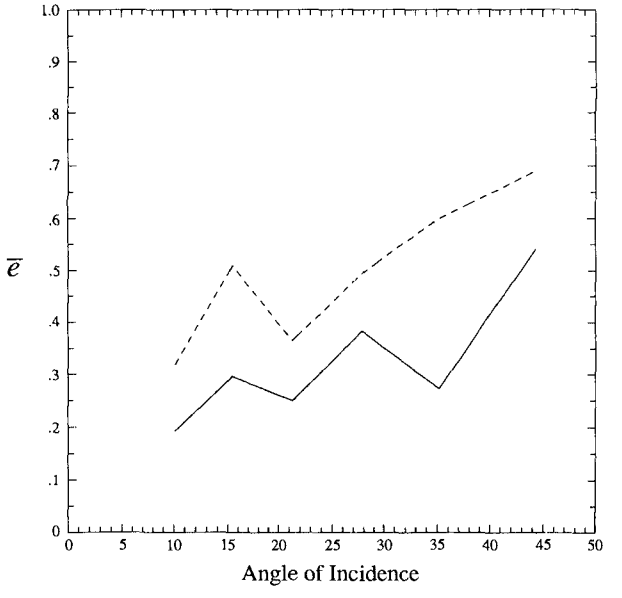

Figure 6: Variation of overall normalized error $\overline{e}$ with angle of incidence β. ——, spectral model; - - -, parabolic model.

hatu performed the parabolic model computations and the parabolic model - data comparisons.

Appendix A: References

Dalrymple, R.A. and Kirby, J.T., 1988, "Models for very wide-angle water waves and wave diffraction", *J. Fluid Mech*, 192, 33-50.

Dalrymple, R.A., Suh, K. D., Kirby, J.T. and Chae, J. W., 1989, "Models for very wide-angle water waves and wave diffraction. Part 2. Irregular bathymetry", *J. Fluid Mech*, 201, 299-322.

Elgar, S. and Guza, R.T., 1985, "Shoaling gravity waves: comparisons between field observations, linear theory, and a nonlinear model", *J. Fluid Mech.*, 158, 47-70.

Elgar, S. and Guza, R.T., 1986, "Nonlinear model predictions of bispectra of shoaling surface gravity waves", *J. Fluid Mech.*, 167, 1-18.

Freilich, M.H. and Guza, R.T., 1984, "Nonlinear effects on shoaling surface gravity waves", *Phil. Trans. Roy. Soc. Lond.*, A 31, 1-41.

Freilich, M.H., Guza, R.T. and Elgar, S., 1990b, personal communication.

Goring, D.G. and Raichlen, F., 1980, "The generation of long waves in the laboratory", *Proc. 17th Intl. Conf. Coastal Engrng.*, Sydney.

Hammack, J., Scheffner, N. and Segur, H., 1989, "Two-dimensional periodic waves in shallow water", *J. Fluid Mech.* 209, 567-589. (referred to in the text as HSS).

Hammack, J., Scheffner, N. and Segur, H., 1990, personal communication.

Kirby, J. T., "A discrete angular spectrum model for nonlinear shallow water waves. Part 1. Waves in laterally uniform domains," submitted to *Journal of Fluid Mechanics.*

Kirby, J. T., 1990, "Intercomparison of truncated series solutions for shallow water waves", submitted to *J. Waterway, Port, Coastal and Ocean Engrng.*

Liu, P.L-F., Yoon, S.B. and Kirby, J.T., 1985, "Nonlinear refraction- diffraction of waves in shallow water", *J. Fluid Mech.*, 153, 185-201. (referred to in the text as LYK)

Peregrine,D.H., 1967, "Long waves on a beach", *J. Fluid Mech.*, 27, 815-827.

Su, C. H. and Mirie, R. M., 1980, "On head-on collisions between two solitary waves", *J. Fluid Mech.*, 98, 509-525.

Yoon, S. B. and Liu, P. L.-F., 1989, "Stem waves along a breakwater", *J. Waterway, Port, Coast. and Ocean Engrng.*, 115, 635-648.